CHAPTER 3

TEG integrated fixed clay stove

3.1. Introduction

Lack of access to clean cooking facility leading to indoor air pollution and drudgery of fuel collection are found as a common feature in rural areas. Traditional fixed clay stoves are associated with low thermal efficiency (<10%) and sufficient heat losses during operation [1-4]. Another feature of rural areas is the lack of access of reliable electricity which leads to dependency on hazardous kerosene lighting.

Fixed clay biomass cook stove will remain predominant in certain pockets as discussed in Chapter 1 and subsequently in Chapter 2. Further, the difficulties faced by a major chunk of population due to non-availability of regular supply of electricity and also due to improper cooking device have elaborately been discussed in Chapter 1. This is a social problem and similar problems are solved through technological interventions. So, intervention of a technology known as thermoelectric generator (TEG) in a fixed clay stove would result in two outcomes in the present context. First, if a fixed clay stove of improved type could be selected for integration of TEG, the acceptance of the TEG integrated cook stove will be increased and second, the thermal energy stored within the stove body could be utilized for electricity generation making the TEG integrated cook stove multifunctional. The prospect of TEG for conversion of different type of heat source into electricity as a proven technology was elaborately discussed in Chapter 2. It is also used for metallic cook stoves which are successfully demonstrated and commercialized. There are many varieties of commercialized TEG integrated stoves enabling to increase the overall efficiency through such integration as well as to convert the stove from a single-use to a multi-functional use. However, limited research and development are noticed in a fixed clay type of cook stove. In a typical Indian context, considering the popularity of fixed clay stove and also considering the prospect of TEG as a proven technology for conversion of heat into electricity, the present research has been undertaken to develop a TEG integrated fixed clay stove.

Keeping in view of the above discussion, the technical feasibility of integrating TEG with a

fixed clay stove to recover, convert and utilize waste thermal energy is investigated. This chapter includes, (i) estimation of thermal energy stored in the stove body, (ii) TEG assembly to recover waste thermal energy, (iii) integration of TEG assembly with fixed clay stove, and (iv) performance testing of TEG integrated fixed clay stove (TIFICS)

In subsequent chapters the results of TEG integrated fixed clay stove deployed in a rural area and users' experience are investigated.

3.2. Conceptualization of TIFICS

The architecture of the TIFICS is comprised of three components viz., (i) improved fixed clay biomass stove, (ii) TEG assembly, and (iii) load system. TEG assembly and load system are assembled and integrated with the improved cook stove to obtain TIFICS. Further, TEG assembly comprises of (a) heat collector (to collect heat from the combustion chamber), (b) TEG module (to convert the collected heat into electricity), and (iii) heat sink (to maintain cold temperature at cold side of TEG). The load system comprises of a battery charging circuit and electrical loads (LED light and mobile phone).

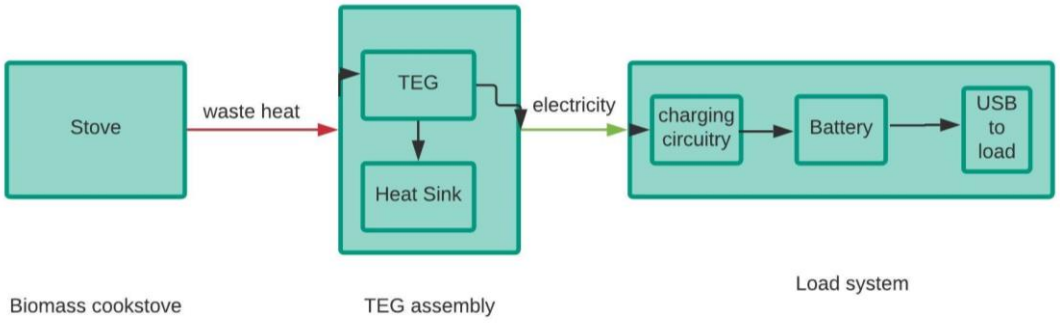

Fig. 3.1 Schematic of TEG integration with fixed clay cook stove (Author's conception)

3.3. Development and performance testing of TIFICS

The procedures involved in the development of TIFICS are illustrated in Fig 3.2. The testing for its performance follows the development and is also shown in Fig. 3.2 and discussed below.

An improved fixed clay stove was selected which is approved and disseminated across India by the Ministry of New and Renewable Energy, India. The details of the cook stove are discussed in Section 3.4. Thermo-physical properties (viz., specific heat, density, thermal conductivity and thermal diffusivity) of the stove material had been determined. The

procedure of determining the thermo-physical properties of the stove through standard experimental procedure is discussed in Section 3.5. The temperature distribution at the inner wall of combustion chamber, flame, fuel bed, flue gas, pot bottom and outer wall of the combustion chamber was assessed during cook stove operation. The temperature distribution on the combustion chamber inner wall was used to determine the location of mounting the TEG assembly to receive sufficient temperature for heat to electricity conversion. Detailed description of selection and measurement procedure is presented in Section 3.6. Assessment of temperature distribution inside the combustion chamber of the stove was useful to estimate heat transfer within the combustion chamber of cook stove using fundamental heat transfer equations and correlations available from the literature. The detailed procedure of measurement is provided in Section 3.7.

The TEG assembly comprised of three components i.e., (i) heat collector, (ii) TEG module and (iii) heat sink. Development procedure of individual components is discussed in Section 3.8. Once the location of mounting was identified, TEG assembly was integrated with the fixed clay stove to obtain TIFICS which is discussed in Section 3.9. The performance of TIFICS was tested under (i) matched load, (ii) light illumination, and (iii) battery charging. The experimental set up and procedure of measurement are presented in Section 3.10.

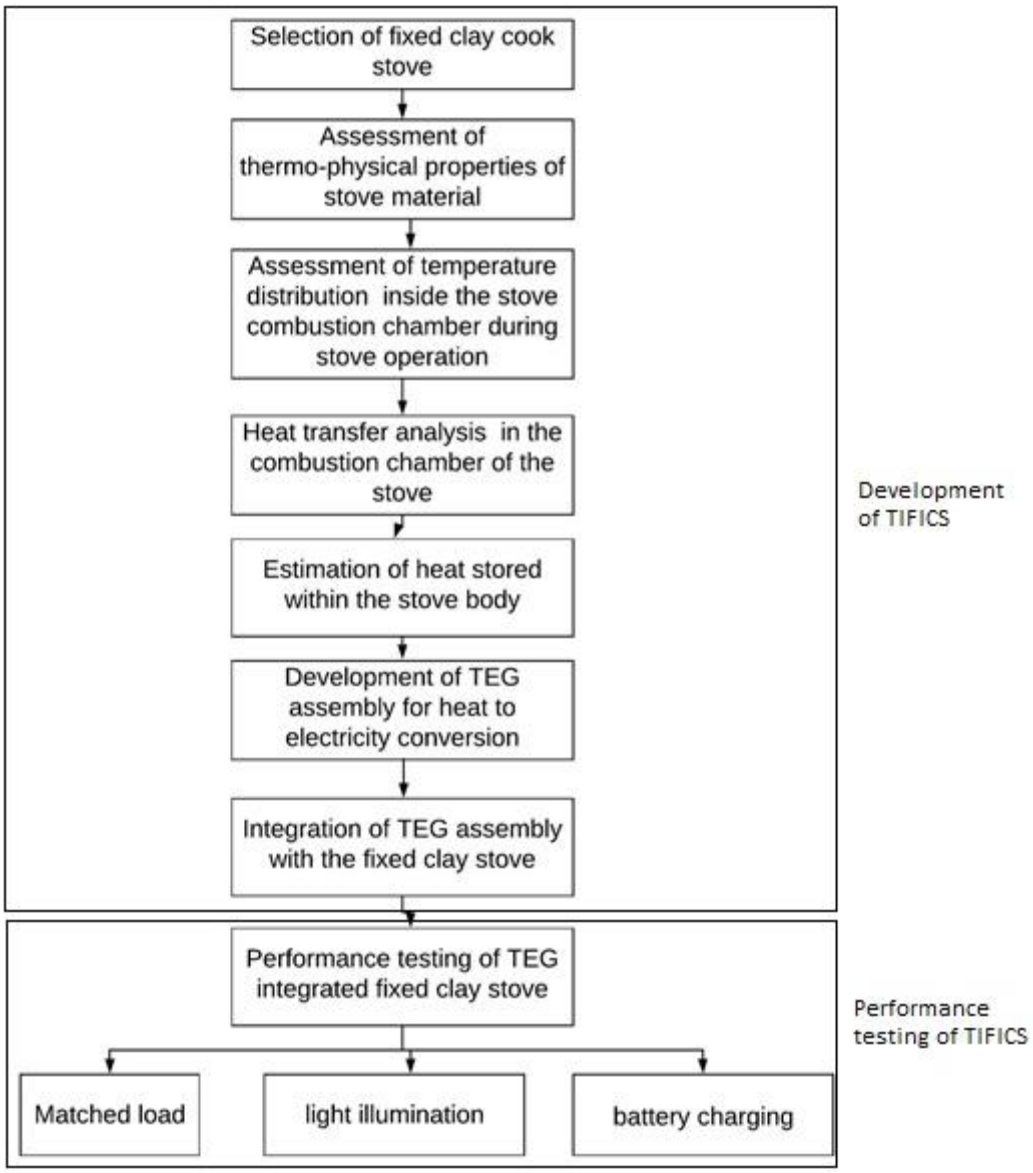

Fig. 3.2 Procedure of development and performance testing of TIFICS

3.4. Selection of fixed clay cook stove

Most of the rural areas in India use fixed clay made traditional biomass cook stove with some variations in their design. Three-stone clay coated stoves were most preferred stove due to ease of construction with locally available material and requiring no special skill to construct. However, some improvised versions of the traditional three-stone stove with an elevated platform for keeping cooking accessories were also used as discussed in Chapter 1. Both the versions lacked chimney for taking the exhaust gas out and therefore, remained as source of

indoor air pollution besides lower thermal efficiency (<10%) [1-4]. There had been several efforts by Government sponsored missions in India to introduce improved cook stove in order to mitigate the problems of indoor air pollution and lower thermal efficiency [4-7]. There are more than 30 proven designs of improved fixed type cook stove which are disseminated with different degree of success.

Sukhad, as shown in Figure 3.3, is a fixed clay improved cook stove approved by the Ministry of New and Renewable Energy, Govt. of India and developed by CTAE, Rajasthan Agricultural University (India) and *Sukhad* had been considered for the present study due to its potential application prospects in the rural areas of India [5]. Success stories of *Sukhad* dissemination were reported in literature where 980 *Sukhad* stoves were distributed in Bundelkhand region, Uttar Pradesh, India under the project entitled, "Energy Services for Village Households and Livelihood Enterprises" [8]. *Sukhad* was also promoted by Assam Energy Development Agency, Government of Assam, India, due to its features matching with the local cooking methods and customs.

The average size of a family in India ranges from 5-8 members and *Sukhad* is suitable for such sized family. Most of rural users use flat or spherical bottom vessels with diameter range between 19 and 30cm which is also supported by *Sukhad*. *Sukhad* is fuel flexible (firewood to agro residues) cook stove and can be constructed with locally available materials such as clay, cow-dung and rice husk. The stove is provided with two pot holders in such a way that the primary pot holder sits above the combustion chamber while the secondary pot holder receives heat from the flue gas generated in the combustion chamber through internally connecting conduit. A chimney takes the exhaust gas out of the cooking and living area through natural draft. The maximum thermal efficiency of *Sukhad* has been reported as 25% with a fuel burn rate of about 1kg/h [5].

Fig. 3.3 *Sukhad* stove

3.5. Thermo-physical properties of stove material

Thermal and physical properties of the fixed clay stove material are required to determine waste heat stored in the stove body. Specific heat (C_p), J/kg.K, thermal conductivity (k_{stove}), W/m.K, density (ρ), kg/m^3, and thermal diffusivity (α_d), m$^{2/}$s are determined.

Specific heat of the stove material was considered as 920 J/kg.K from reported literature [9]. Whereas, thermal conductivity was measured through experiment and thermal diffusivity is estimated using Eq. 3.2.

Thermal conductivity of stove material was estimated from one dimensional steady state heat conduction method as shown in Fig. 3.4. A sample of stove material from *Sukhad* stove was shaped into a dimension as shown in Fig. 3.4. The well-defined sample of stove material was stacked in series with an aluminum plate of known thermal conductivity ($k_{aluminum}$) and similar dimension as the sample. The entire stack was placed over a hot plate in such a way that aluminum plate faces the hot plate and the stove material was exposed to ambient air. Three calibrated *K-type* thermocouples (T1, T2 and T3) were placed at the interfaces as shown in Fig. 3.4. The interfaces was assumed to have uniform contact. The hot plate was set to a temperature of 60ºC as presented in literature [9]. The assembly was allowed to reach steady state and temperature was recorded at each interfaces. Assuming one dimensional heat flow, the unknown thermal conductivity of the stove material (k_{stove}) was estimated using Eq. 3.1.

$$Q'' = \frac{k_{aluminum}(T_1 - T_2)}{L_1} = \frac{\boldsymbol{k_{stove}}(T_2 - T_3)}{L_2} \quad (3.1)$$

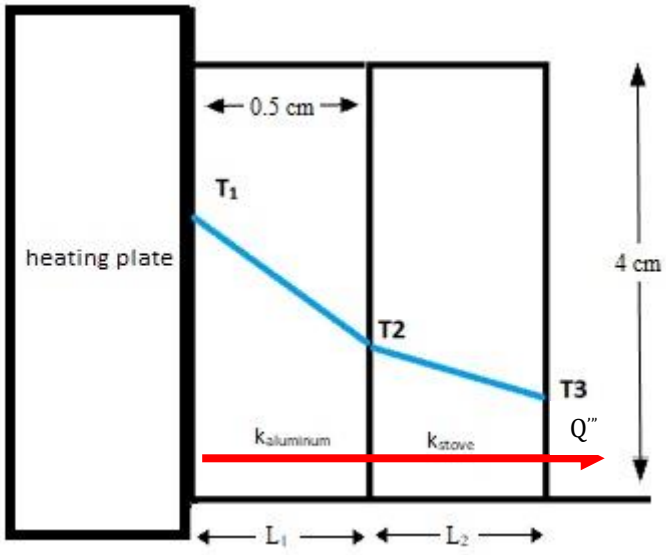

Fig. 3.4 One-dimensional heat conduction method

Density of the stove material (ρ) was estimated by measurement of a known volume and mass of the stove material. The test was repeated three times.

Thermal diffusivity (α_d) of the stove material was determined in order to know the rate of heat transferred from hot side of the stove body i.e. the CC inner wall to the cold side of the stove body i.e. the CC outer wall and it was calculated from Eq. 3.2, which depends on the three parameters i.e. density, specific heat and thermal conductivity.

$$\alpha_d = \frac{k_{stove}}{\rho C_P} \quad (3.2)$$

3.6. Temperature distribution inside combustion chamber of fixed clay stove

Series of experiments (ten replications) were conducted with cooking pot on top of the combustion chamber to assess the temperature on key locations inside the combustion chamber of the *Sukhad* stove using a representative fuel wood (*Azadirachta indica*, local name: *Neem*) at a fuel feed rate of 16.67g/min (100g/6min) as per the BIS standard [10]. An aluminium pot with 6L of water was placed over the combustion chamber during the experiment. Each experiment was spanned over one hour of stove operation considering the fact of a typical cooking cycle in Indian households' i.e. 1h. Thirteen *K-type* thermocouples were mounted at 13 locations to measure temperature during operation of the stove. Five out of 13 thermocouples were mounted to record temperature of fuel bed, flame, pot bottom, stove outer body and flue gas temperature. The flame temperature was measured at a height

of 3/4th of the height of combustion chamber [11]. The length and height of the combustion chamber inner wall is 30cm and 18cm, respectively. The remaining eight thermocouples were mounted on inner wall of the combustion chamber at uniformly distributed locations (on the bed and at 9cm above bed spanning at four angular locations) as depicted in Fig. 3.5.

Division of the surface for temperature measurement at the inner wall of the combustion chamber through uniform rectangular grid is shown in Fig 3.5(c), Dimension of each rectangular grid was set at 4.5cm and 5cm as shown in Fig. 3.5(c). Each grid area was assumed to be a representative temperature of the locations of temperature measurement. The temperature distribution along this grid enabled to identify the location for mounting TEG assembly.

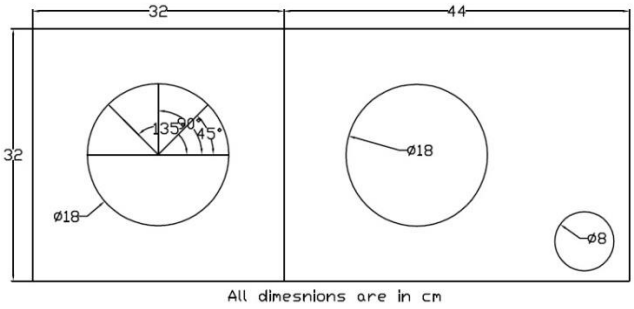

(a)

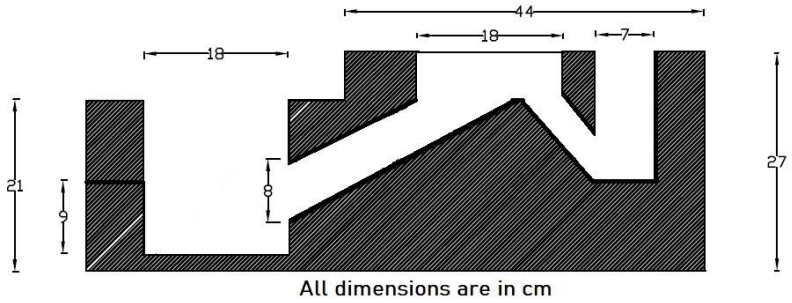

(b)

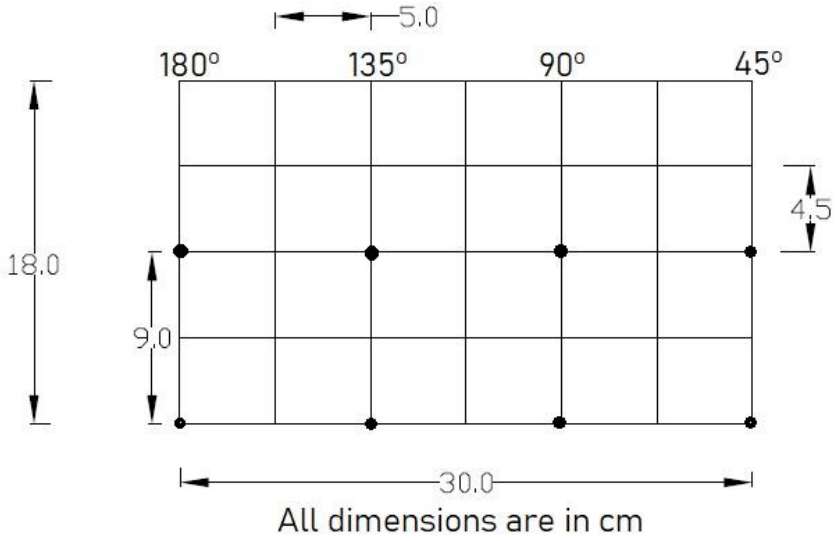

(c)

Fig. 3.5 Indicative layout of the stove inner wall with identified locations for temperature measurement: (a) top view showing angles in degree from a reference plane and (b) front view showing height in cm from the bed (c) projected view of inner wall of combustion chamber

3.7. Heat transfer estimation inside CC of the stove

Heat transfer to the CC inner wall from the fuel bed ($Q_{fb.cc}$), flame ($Q_{flame.cc}$), and flue gas ($Q_{conv,g}$), heat stored in the CC wall (Q_{stored}), and heat transferred from the CC wall to pot (Q_{cc_potB}) and ambient air (Q_{o_amb}) was determined as illustrated in the Fig 3.6. Each component of heat transfer was individually estimated. The detailed procedure of heat transfer analysis is mentioned below.

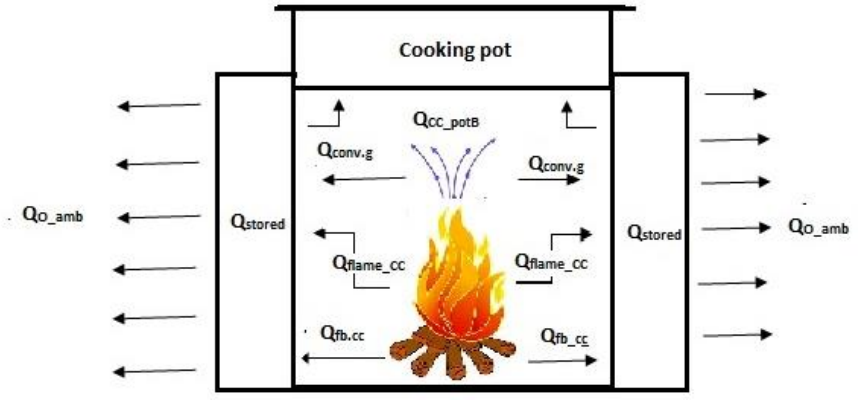

Fig. 3.6 Heat transfer inside combustion chamber

The equations (Eq. 3.3 to Eq. 3.11) used to estimate heat transfer inside the stove was used for a different set of stoves. The fundamental relations can also be used for the present case. However the parameters used in the relationships were re-estimated pertaining to the present case.

3.7.1. Heat transfer from fuel bed to CC inner wall

Fuel bed transfers radiative heat at temperature, T_{fb} to CC inner wall at $T_{w,i.}$ which was determined using the equation [11] shown below

$$Q_{fb.cc} = F_{fb.cc} \times A_{fb} \times \epsilon_{fb} \times \sigma \times (T_{fb}^4 - T_{w,i}^4) \quad (3.3)$$

where $F_{fb.cc}$, A_{fb}, ε_{fb}, σ, T_{fb} *and* $T_{w,i}$ are the view factor from fuel bed to CC, area of fuel bed, emissivity of fuel bed, Stefan-Boltzmann's constant, fuel bed temperature and CC inner wall temperature, respectively. View factor and area were calculated whereas, emissivity of the fuel bed is assumed from a reported literature [11] and Stefan Boltzmann's constant is a known constant shown in Table 3.1.

Table 3.1 Fuel bed Properties

Parameter	Value	Remarks
$F_{fb.cc}$ (view factor from fuel bed to CC inner wall)	0.94	Calculated
Area of the fuel bed (A_{fb}) m^2	0.02543	Calculated
Emissivity of fuel bed(ε_{fb})^	0.8	[11]
σ , $W/m^2.K^4$	5.67×10^{-8}	-

3.7.2. Heat transfer from flame to CC inner wall

During operation of the stove, the combustion chamber inner wall was exposed to the flame and radiated heat was received from the flame at T_{flame} which is evaluated using Eq. 3.4 [11].

$$Q_{flame.cc} = F_{flame.cc} \times A_{flame} \times \epsilon_{flame} \times \sigma \times T_{flame}^4 \times (1 - exp^{-kx}) \quad (3.4)$$

where, $F_{flame.cc}$, A_{flame}, ϵ_{flame}, σ, T_{flame}, k and x are the view factor from flame to combustion chamber inner wall, area of the flame, emissivity of flame, Stefan-Boltzmann's constant, flame temperature, decay coefficient of the flame and thickness of the flame, respectively. View factor of flame to CC inner wall was calculated as view factor of base to a finite cylinder [17, 18]. Flame exposed area was the area of the CC inner wall. Flame thickness is equal to the fuel bed length of breadth which in the present case is the diameter of the fuel bed [11]. The flame properties are shown in Table 3.2.

Table 3.2 Flame properties

Parameter	Value	Remarks
$F_{flame.cc}$ (view factor of flame to CC inner wall)	1	Calculated
Area of the flame (A_{flame}) m^2	0.076	Flame exposed area
Emissivity of flame(ε_{flame})	0.31	[11]
σ , $W/m^2.K^4$	5.67×10^{-8}	-
k (decay coefficient), m^{-1}	0.7322	[11]
x (flame thickness), m	0.18	Calculated

3.7.3. Heat transfer from flue gas to CC inner wall

In addition to flame and fuel bed, the flue gas flowing inside the CC at T_g transfers convective heat to the CC inner wall at $T_{w,i}$, which was determined using the following equation

$$Q_{conv,g} = h \times A \times (T_g - T_{w,i}) \quad (3.5)$$

where, T_g, h and A are the temperature of flue gas, convective heat transfer coefficient of flue gas to CC inner wall and area of the CC inner wall.

Several researchers have reported the flow inside a natural convection cook stove as laminar and thus laminar flow governing equations are sufficient to determine convective heat transfer coefficient [12-14]. Thus, the convective heat transfer coefficient (h) of flue gas to the combustion chamber inner wall was estimated similar to the calculation of h inside a tube for laminar flow [15] and shown in the equation below.

$$h = \frac{4.36 \times k_g}{D_{cc}} \tag{3.6}$$

where, k_g is the thermal conductivity of the flue gas, W/m.K and D_{cc} is the diameter of the CC.

Flue gas follows the behaviour of ideal gas and thermal conductivity (k_g) of flue gas is same as that of air evaluated at atmospheric pressure and thus correlation of thermal conductivity of air in temperature (T) range of 27-1200ºC was used as shown in Eq.3.7 [16].

$$k_g = 0.00031847 \times T^{0.7775} \tag{3.7}$$

3.7.4. Heat transfer from combustion chamber inner wall

Heat transfer from CC inner wall takes place in the form of radiation to pot bottom of diameter 0.24m and conduction to CC outer wall. The pot bottom receives radiative heat (Q_{cc_potB}) from CC inner wall. As presented in the literature [11], the calculation of heat transfer from CC inner wall to pot bottom was determined as,

$$Q_{cc\_potB} = F_{cc\_potB} \times A_{cc} \times \epsilon_{cc} \times \sigma \times (T_{cc}^4 - T_{potB}^4) \tag{3.8}$$

where, F_{cc_potB} is the view factor from CC inner wall to pot bottom surface, A_{cc} is the combustion chamber inner wall area, ϵ_{cc} is the emissivity of CC inner wall, T_{cc} is the CC inner wall temperature and T_{potB} is the pot bottom temperature.

It is important to mention that the area of the outer wall of combustion chamber was considered for calculation heat loss to ambient conditions as shown in Fig. 3.7. Convection and radiation heat loss from the secondary pot section was negligible since the section mostly remains at temperature close to ambient condition.

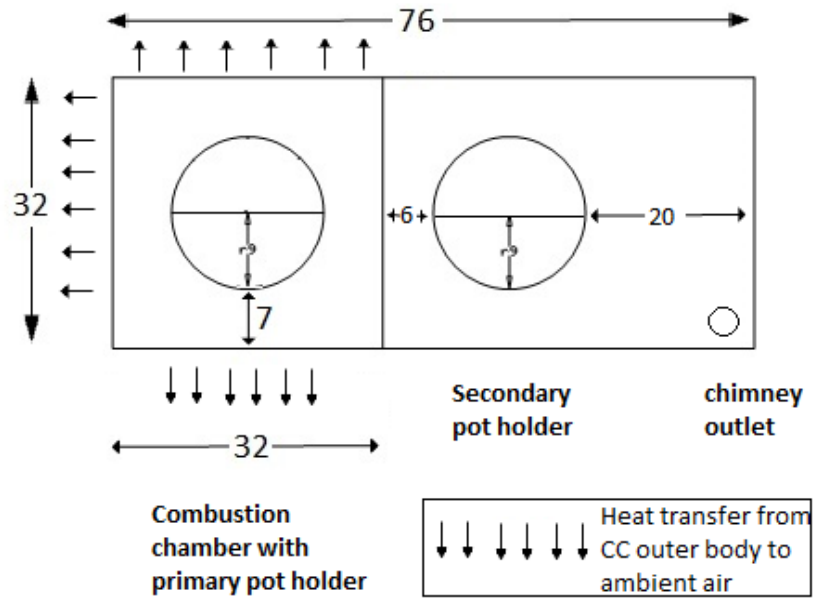

All dimensions are in cm

Fig. 3.7 Schematic of heat loss from CC outer wall

Heat transfer form combustion chamber outer wall to ambient air takes place through radiation and convective mode which is obtained from [11] and was determined using Eq. (3.9).

$$Q_{o\_amb} = h_{amb} \times A_0 \times \left(T_{w,o} - T_{amb}\right) + \{\varepsilon_{stove\ wall} \times \sigma \times A_o \times ({T_{w,o}}^4 - {T_{amb}}^4)\} \quad (3.9)$$

where, h_o, A_o, $T_{w,o}$, $T_{a,}$ $\varepsilon_{stove\ wall,}$ σ are the heat transfer coefficient for the outer wall, area of CC outer wall, outer wall temperature, ambient temperature, emissivity of outer wall and Stefan-Boltzmann's constant, respectively.

Ambient air flows over the surface of combustion chamber outer wall. Thus, the convective heat transfer coefficient, h_{amb} for the outer CC outer wall was calculated using empirical relation of Nusselt Number (Nu_L), Rayleigh Number (Ra_L), Prandtl Number (Pr) [15], which is:

$$Nu_L = \left\{ 0.825 + \frac{0.387\, Ra_L^{\frac{1}{6}}}{\left[1+\left(\frac{0.492}{Pr}\right)^{\frac{9}{16}}\right]^{8727}} \right\}^2 \quad (3.10)$$

$$h_{amb} = \frac{Nu_L . k_{amb}}{L} \quad (3.11)$$

Where, k_{amb} and L are the thermal conductivity of ambient air, and Length of air contact of the CC outer wall. Thermal conductivity of ambient air was determined using Eq. 3.7. The length of air contact of CC outer wall is assumed to be the height of the wall. Prandtl number of air at ambient temperature was considered i.e. 0.71 [15].

3.7.5. Heat absorbed by the CC inner wall

Determination of the amount of heat absorbed the stove body is dependent upon the thermal and physical properties of stove material. The following equation was used to calculate the heat absorbed by the stove [3].

$$Q_{stored} = 2 \times k_{stove} \times A_{cc} \times \left(T_{w,i} - T_a\right)(\pi \times \alpha_d \times 3600)^{-0.5} \quad (3.12)$$

where, k_{stove}, A_{cc}, $T_{w,i}$, T_a, α_d, are thermal conductive of stove material, area of CC, CC inner wall temperature, ambient air temperature and thermal diffusivity of the stove material.

3.8. Development of TEG assembly

As discussed earlier, TEG assembly comprises of heat collector, TEG module and heat sink. The procedure of development of each component along with its integration is discussed below.

3.8.1. Heat collector plate

Temperature distribution on the inner wall of CC was used to identify the location of the heat collector plate. Three materials viz., copper, aluminium, and stainless steel (SS404) were chosen and compared for suitability as a collector plate based on thermal conductivity, strength to weight ratio and unit cost. Higher thermal conductivity was preferred for quick dissipation of heat to the TEG module. There should be a balance between the soundness of the technology and its cost which governs the affordability vis-à-vis acceptability. User affordability of the technology is related with the cost of production. Therefore a cheaper

material was preferred for the heat collector plate. The best material was selected combining all the three criteria which are discussed above.

The dimension of the heat collector plate was determined based on the available surface area having sufficient temperature to capture heat.

After selecting the best material for heat collector plate, temperature distribution during stove operation was investigated with the plate of the material. The information of temperature distribution was used to select the suitable thermoelectric generator (TEG) module.

3.8.2. TEG module

There are several commercially available TEG modules, making the selection of appropriate TEG module critical for the present study. A total of 15 commercialized TEG module from different manufacturers were compared on the basis of (i) peak hot side temperature (ºC), (ii) load voltage (V), (iii) output power (W), (iv) output current (A), and (v) cost/Watt power produced (US$/W).

The temperature inside the combustion chamber was expected to be high (>500ºC) [10, 12-14], The TEG module that can withstand high temperature without damage was preferred. Power output in the range of 7-8W was expected to fulfil user need for illumination and battery charging. Load voltage of 6V was considered for TEG selection as most of the basic electrical appliances (LED light, mobile phone and other battery powered devices) requires a minimum operating voltage of 5V. Further, LED bulb in the range of 3-6W of power rating provides adequate illumination level in a working space. Higher the flow of current, quicker the time to charge a battery powered device. Therefore, a TEG module with peak output current in the range of 1-1.5A was considered as the criteria. The cost of the TEG module was another criteria which determines the affordability. Lower unit cost (US$/Watt) was preferred for TEG module selection. Finally, based on the criteria, best TEG module was selected.

3.8.3. Heat sink

As elaborately discussed in Chapter 1 and Chapter 2, four modes of cooling based on type of convection and type of fluid used in cooling were used to cool the heat sink attached to the cold side of TEG module [19-29]. These are (i) natural convection air cooling (NCA), (ii) natural convection water cooling (NCW), (iii) Forced convection air cooling (FCA) and (iv) Forced convection water cooling (FCW).

Selection of an effective heat sink to ensure proper cooling system was desired as for a given hot side temperature, lower the cold side temperature better will be the performance. The appropriate cooling system was preferred on the basis of (i) external power required for operation, (ii) thermal resistance to heat flow, (iii) prospect of utilization of rejected heat, and (iv) minimum and maximum temperature achievable. These information were obtained from literatures which were reviewed and the best cooling technology suitable for the present study was selected.

As far as material for heat sink is concerned, identical criteria as considered for heat collector plate were used.

3.9. Integration of TEG assembly with fixed clay stove

Heat collector plate, TEG module and heat sink were assembled with fasteners to obtain TEG assembly. A groove to accommodate the TEG assembly on the inner wall of the combustion chamber was made and the TEG assembly is press fitted with appropriate locking device to prevent dislocation.

3.10. Experimental set up for performance testing of TIFICS

The performance testing of TIFICS was assessed under three mode of operation viz. matched load, LED illumination and battery charging.

The TEG module is regarded as a DC power source. A load matching the internal resistance of the TEG module was connected as shown in Fig 3.8. The setup was equipped with data logger (Make: IOTech Personal Daq56) for temperature and voltage measurements. Four *K*-type thermocouples (connected to the data logger) as shown in Figure 3.8 were mounted to record the temperatures at (i) hot side of the TEG module, (ii) cold side of the module, (iii) flame of combustion, and (iv) ambient air. The hot side and cold side temperature readings were used to determine the temperature difference across the TEG module. Voltage was measured at the output of TEG module (V_{TEG}) and drop across the matched load (V_R) was measured as shown in Fig. 3.8. The current (I_R) flowing through the load resistance was calculated using Ohm's law and output power was determined from the product of TEG output voltage and current.

The recording of data (temperature and voltage) was spanned over a typical cooking cycle i.e. 1h following the standard reported in earlier researches [25-29]. Data recording was done at an interval of 30 seconds during the cycle of the stove operation. Fuel wood (*Azadirachta*

indica, local name: *Neem*) was fed at the rate of 16.67g/min (i.e.100g/6min) in batches spanning over 6 min as per the standard stove testing protocol of Bureau of Indian Standards [10].

Thirty hours of tests were carried out to investigate the production of power (W) with respect to temperature difference. Electrical energy generation (Wh) was estimated by integrating power duration curve.

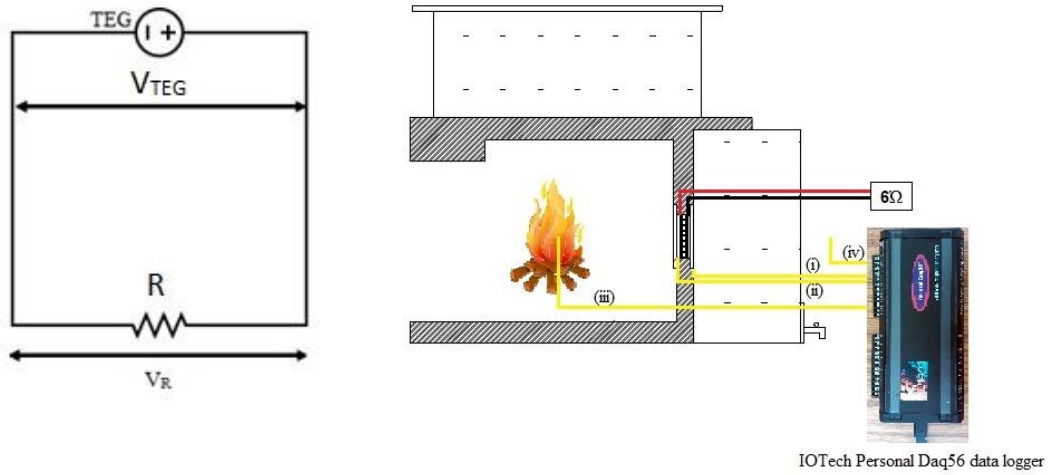

Fig. 3.8 TIFICS with matched load

In the second mode of operation, the LED was connected to the output terminal of the TEG module. The duration of illumination of the LED bulb was recorded for a typical cooking cycle of TIFICS operation.

The capability of the TIFICS was also assessed to re-charge a battery so that it can behave as a backup power source for LED illumination and mobile phone charging. Selection of a suitable battery to be charged by TEG was an important consideration for the present study and was dependent upon the quality and amount of voltage and current produced by the TEG during TIFICS operation.

Five types of batteries viz., (i) Lithium iron phosphate ($LiFePO_4$), (ii) Lead acid, (iii) Nickel Cadmium (NiCd), (iv) Nickel metal-hydride (Ni-MH), and (v) Lithium cobalt oxide ($LiCoO_2$) were selected based on battery density, operating temperature range, life cycle, safety and impact on environment. These information were obtained from battery manufacturers. The best battery among the shortlisted batteries was used to be charged by TIFICS.

Before charging, the battery was discharged to its cut-off voltage using a LED bulb. Once the battery was discharged to its cut-off voltage, the battery was connected to the TEG module till the point when it reached its full charged voltage (as specified by the manufacturer). Series of ten replicated tests were conducted to investigate the charging time required to fully charge the battery using TIFICS.

3.11. Results and Discussion

3.11.1. Thermo-physical properties of stove material

Thermal conductivity of the stove material was estimated to be 0.9W/m.K. The stove material was made of clay with additives of cow dung (20%) and rice husk (5%) on weight basis. The thermal conductivity of cow dung (0.09W/m.K) and rice husk (0.03W/m.K) clearly had an influence on the overall low thermal conductivity of stove material [30, 31]. When compared with thermal conductivity of metallic stove material such as stainless steel (14W/m.K), aluminium (250W/m.K) and cast iron (45W/m.K) of other improved cook stoves [32], it was very less. The low thermal conductivity signifies that heat transferred on the combustion chamber inner wall would be dissipated in a sluggish manner to its outer wall. Thus, a possibility of heat absorption during stove operation was expected.

Comparing specific heat of stove material (920J/kg.K) with common metals of improved cook stove such as aluminium (780J/kg.K), cast iron (462J/kg.K) and stainless steel (468J/kg.K), it was evident more heat was required to raise the temperature of stove body compared to other metals [33].

The average density of three replicated tests of stove material was estimated to be 1469kg/m^3. Thermal diffusivity was calculated and found to be 6.65 $\times 10^{-7} m^2/s$ which was very small compared to aluminium ($6.4\times10^{-5} m^2/s$), stainless steel ($1.17\times10^{-5} m^2/s$) and cast iron ($2.3\times10^{-5} m^2/s$) which signifies that rate of heat transfer of the stove material from the hot end to cold end is slow [34]. The thermal properties indicated that there was a possibility of heat trapping or storing during operation of the stove.

3.11.2. Temperature distribution inside the combustion chamber

The temperature of the combustion chamber inner wall is plotted against time of stove operation and shown in Fig. 3.9. Variation of temperature with time can be seen at all the locations probably due to variation of rate of combustion which was inherent feature of biomass type solid fuel [35, 36].

The stove was tested from cold start and therefore, transient heat transfer process might have resulted in higher degree of temperature fluctuations during initial period (~25min). Temperature at all the locations was below 300ºC during the initial period which however increased after the fuel supply increased. The temperature at all the locations stabilized after the 25 min of stove operation and for most of the time (>35 min) stayed at temperature above 300ºC. As mentioned earlier, temperature was recorded at the bed as well as at 9cm above the bed of combustion chamber. Temperature at the bed (i.e. 0cm) with a variation between 400 and 600ºC were found more than at 9cm above fuel bed (300-450ºC).

The values were used for identifying the appropriate mounting position of the TEG assembly considering the safe limit of TEG module. Higher hot side temperature was better for achieving better output of TEG. It is observed from Fig. 3.9, that sufficient temperature in the range of 300-600ºC was available for heat to electricity conversion.

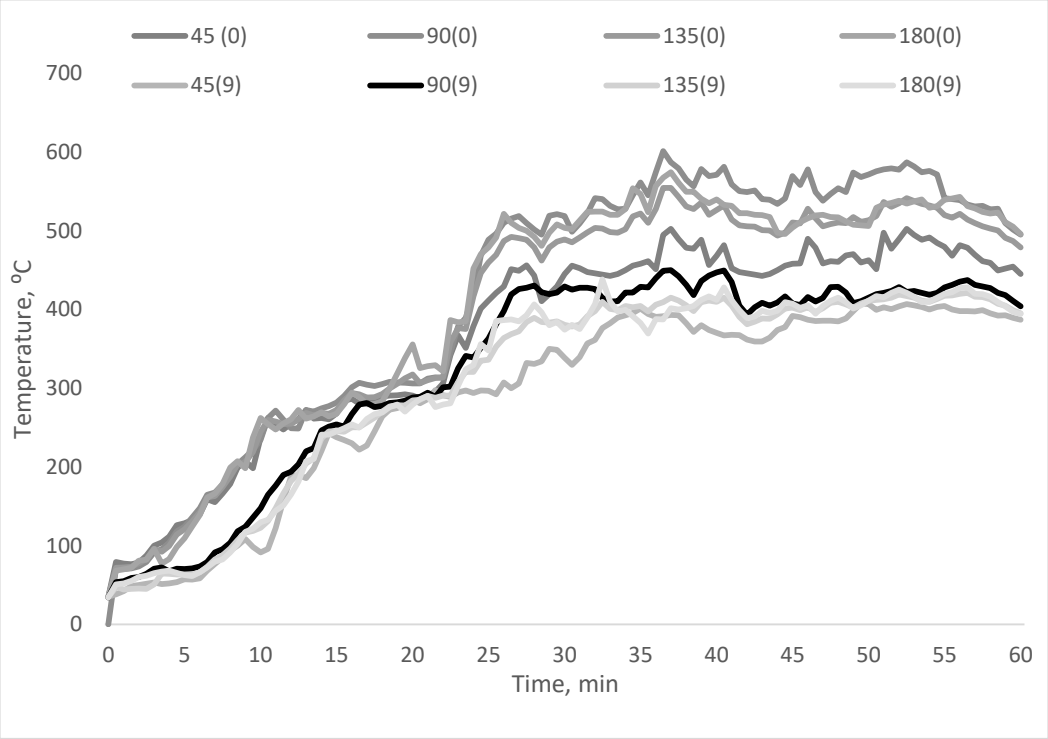

Fig. 3.9 Temperature distribution of the combustion chamber inner wall

3.11.3. Heat transfer inside combustion chamber

Heat transfer inside the combustion chamber was determined as per the fundamental heat transfer relations discussed in Section 3.7. The steady state temperature values at specified

locations were used to determine the various heat transfer components. Flame was recorded to be 770ºC at steady state and it transferred 324W of heat through radiation to the combustion chamber inner wall at 377ºC. The CC inner wall (377ºC) received 426W of radiative heat from fuel bed (578ºC). The flue gas inside the combustion chamber at 501ºC transferred convective heat of 221W to the CC inner wall at 377ºC with 14.88 $W/m^2.K$ convective heat transfer coefficient under natural draft. Overall, 971W of heat was received by the CC inner wall from flame (324W), fuel bed (426W) and flue gas (221W) through radiation and convection. The CC inner wall behaved as a gray surface and transferred heat to pot bottom and CC outer wall. CC inner wall transferred radiative heat of 28W to pot bottom (107ºC). The CC outer wall which was at 60ºC transferred 20W of heat to ambient air at 30ºC through radiation and convection. Heat absorbed by the CC inner wall was 604W during the operation of the stove. The low thermal conductivity stove material (0.9W/m.K) and low thermal diffusivity ($6.65\times10^{-7}m^2/s$) indicated that heat transferred from the CC inner wall at 377ºC to CC outer wall at 60ºC took place at a slow rate during the operation of the stove. The amount of heat stored inside the stove CC inner wall dissipated at a slow rate to the outer body.

3.11.4. Heat collector plate

Inner wall of the combustion chamber of the fixed clay stove provided a cylindrical surface (18cm diameter and 18cm height over fuel bed) for mounting the heat collector plate. From Fig. 3.9, temperature at angular position of 90º at 9cm above the fuel bed offered temperature range between 300 and 450ºC. The temperature range was suitable in the context of mounting TEG module as most of commercialized TEG modules operate in the range of 300-400ºC. Further, from Fig. 3.10 and as mentioned in Section 3.6, the segments around each location of temperature measurement resembled similar temperature. Therefore, the segments around the angular position of 90º at 9cm above fuel bed of dimension 10cm × 9.5cm was considered for mounting the heat collector plate.

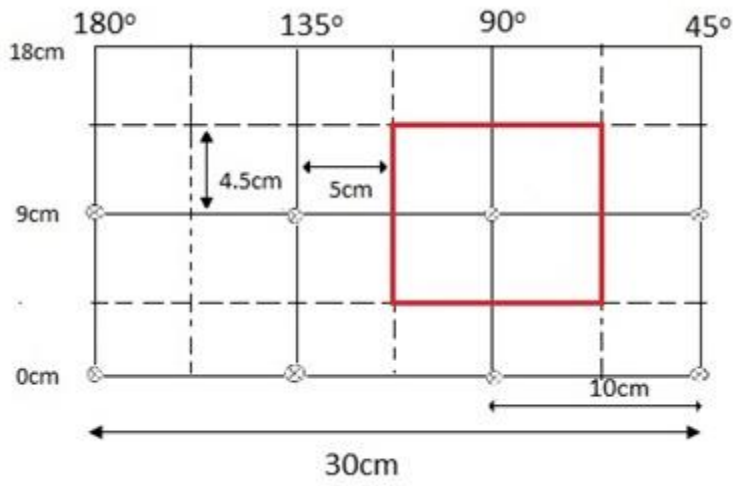

Fig. 3.10 Location for mounting heat collector plate

Table 3.3 details the comparison of materials for heat collector plate. Copper is the highest thermal conductivity material with 388W/m.K compared to aluminium and stainless steel. However, its specific strength is lower compared to the other materials. SS304 is a poor thermal conductivity material as compared to copper and aluminium, but its cost is lower compared to copper and have strength to weight ratio more than copper (24.7). Aluminium is a better thermal conductivity material compared to SS304, but inferior to Copper. However, when strength to weight ratio and cost/kg was considered, it is better compared to both copper and SS304. Based on this discussion, aluminium was selected as the heat collector material. In view with the discussion of location of mounting and material selection, aluminum plate of dimension 10cm × 10cm × 0.2cm was mounted covering the angular position of 90º.

Table 3.3 Material comparison for heat collector plate

Material	Thermal conductivity, W/m.K	Strength to weight ratio (kN.m/kg)*	Cost/kg (US$/kg)	Reference
Copper	388	24.7	5.7	[32]
Aluminium	250	115	1.8	[32]
Stainless Steel (SS304)	14	63.1	3.7	[32]

The developed heat collector aluminum plate was mounted at the selected location and temperature was recorded during operation of the stove. The temperature of the surface of

the aluminum plate is plotted and shown in Fig. 3.11. Temperature in the range of 250-400ºC was available after 15min of stove operation which was suitable for TEG module operation.

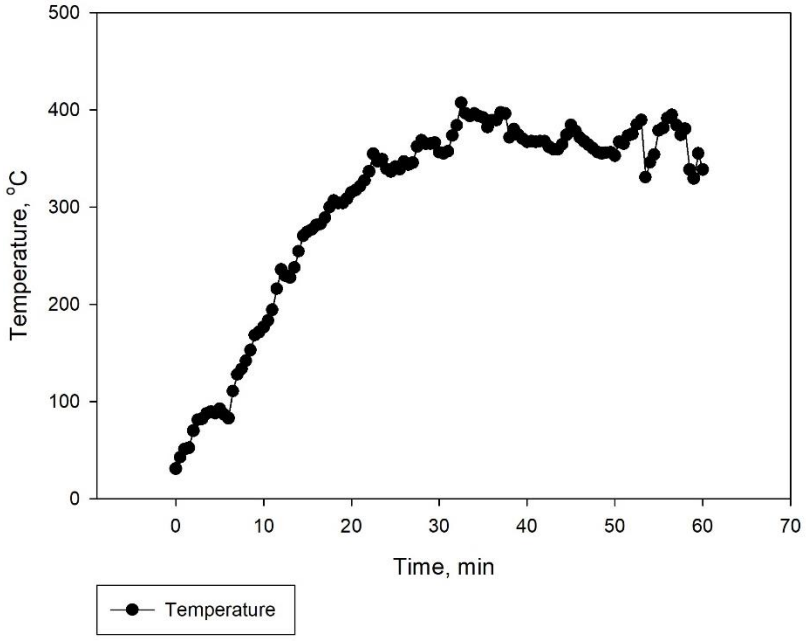

Fig. 3.11 Temperature distribution of the aluminium hear collector plate

3.11.5. TEG module for TEG assembly

Fifteen commercialized TEG modules were compared (Table 3.4) based on the criteria as mentioned in Section 3.8.2. These modules were of uniform dimension i.e. 4cm × 4cm × 0.3cm. Further, from the Figure 3.11, it was observed that a peak temperature variation in the range of 250-400ºC was available on the surface of the aluminum plate. From the Table 3.4, almost every TEG module was capable of operating at a temperature of 300ºC except for Hz2 and Hz9. However, TEP1-1994-3.5 (Serial number 14) was capable of operating at 330ºC and intermittently at 400ºC. Load voltage of 6V and higher was only available with TEG1-4199-5.3 and TEP1-1994-3.5. It is important to notice that both these modules also have identical output power and current which meet the requirement of the present study. However, Hz9 provides an output power of 9W but at low voltage and sufficiently higher cost compared to TEG1-4199-5.3 and TEP1-1994-3.5. If cost/Watt of power produced is observed, TEP1-1994-3.5 is better. Hence, for the present study TEP1-1994-3.5 was chosen for majority of benefits in comparison to the other modules.

Table 3.4 Comparison of commercialized TEG modules

SN	TEG module [Source]	Peak hot side temperature, ^{o}C	Load voltage, V	Output power, W	Output current, A	Cost/W, US$/W
1	Hz2 [37]	230	3.3	2.97	0.81	9.96
2	Hz9 [38]	230	3.2	9.00	2.82	4.34
3	TEP1-1264 1.5 [39]	300	4.7	7.80	1.67	4.67
4	TEC12706 [40]	100	2.0	2.00	1.01	2.88
5	TEG1-4199-5.3 [41]	300	6.7	7.8	1.17	5.02
6	TEG1-12610-4.3 [42]	300	5.3	5.30	0.99	7.15
7	TEG1-12610-5.1 [43]	300	3.9	5.07	1.30	4.98
8	TEG1-1268-4.3 [44]	300	5.3	5.30	0.99	5.65
9	TEG1-1263-4.3 [45]	300	5.3	5.30	0.99	4.82
10	TEP1-12635-3.4 [46]	300	5.4	5.40	1.00	5.29
11	TEP1-1265 1.5 [47]	300	4.7	7.89	1.68	4.67
12	TEP1-1264 3.4 [48]	300	5.4	5.40	1.00	5.01
13	TEG1B-12610-5.1 [49]	250	3.6	7.20	2.00	6.06
14	TEP1-1994-3.5 [50]	330	6.8	7.83	1.17	3.83
15	TEG2-07025HT-SS [51]	190	2.0	6.8	3.4	5.29

3.11.6. Heat sink

Cooling technologies for heat sink were compared and shown in Table 3.5. NCA is basically metal finned heat sinks which is cooled by buoyant forces of cooling air. FCA is a similar metal dinned heat sink but uses a DC powered fan to cool the heat sink, NCW is essentially

a water storage tank or a water reservoir and FCW is a plate with water channel using pumping power for water flow.

There are literatures that have reported that NCA offers high thermal resistance to heat flow [20, 21]. Further, for FCA and FCW, external power is required to operate the cooling process which is either consumed from the produced electrical power from TEG or from an external power source. Thus, the entire produced power is not utilized.

In NCA and FCA there is a possibility of cold side of the TEG to attain temperature similar to hot side temperature. But in NCW and FCW, where water is used as a cooling fluid, the maximum temperature reached in the boiling point of water. There is also a prospect of utilizing the dissipated heat in the form of hot water for domestic purposes. Considering the facts above, NCW was considered over others for the fact it do not uses external power and prospect of utilizing rejected heat as hot water.

As shown in Table 3.3, aluminium was better material compared to copper and stainless on the basis of strength to weight ratio and cost. Although thermal conductivity of aluminium (250W/m.K) is less than copper (388W/m.K), heat conduction will be similar for material with small thickness. Thus, aluminium was selected as the heat sink material.

In the present study, a water storage tank of 2L capacity which signifies the principle of NCW is used. A water storage tank of dimension 20cm × 10cm × 10cm to fill 2L of water was developed. One side of the tank was used to attach the cold side of the TEG module. An outlet valve was attached with the tank for provision of hot water for drinking purpose.

Table 3.5 Comparison of cooling technology for heat sink

Heat sink cooling	Thermal resistance to heat flow	External power consumption	Maximum temperature achieved	Possibility of utilization of rejected heat
NCA	High	No	TEG hot side	No
FCA	Low	Yes	TEG hot side	No
NCW	Low	No	100ºC	Yes (hot water)
FCW	Low	Yes	50ºC	Yes (hot water)

3.11.7. Assembling heat collector, TEG module and heat sink

The selected TEG module had a maximum operating temperature of 330ºC but the temperature available on the heat collector plate was more than the (>330ºC) safe limit of TEG module after 20 min of stove operation as seen from the Fig.3.11. In order to protect the TEG from fluctuating high temperate above the safe limit of TEG, two aluminum plates were used between which the TEG module was clamped.

The size of the TEG module was 4cm × 4cm × 0.2cm and was clamped between two 6cm × 6cm × 0.3cm aluminium plates with fasteners as shown in Fig. 3.12 and 3.13. The hot side of TEG module was attached to one surface of the heat collector plate and the cold side was attached to the water storage tank. The other surface of the heat collector plate was exposed to heat of combustion inside the combustion chamber.

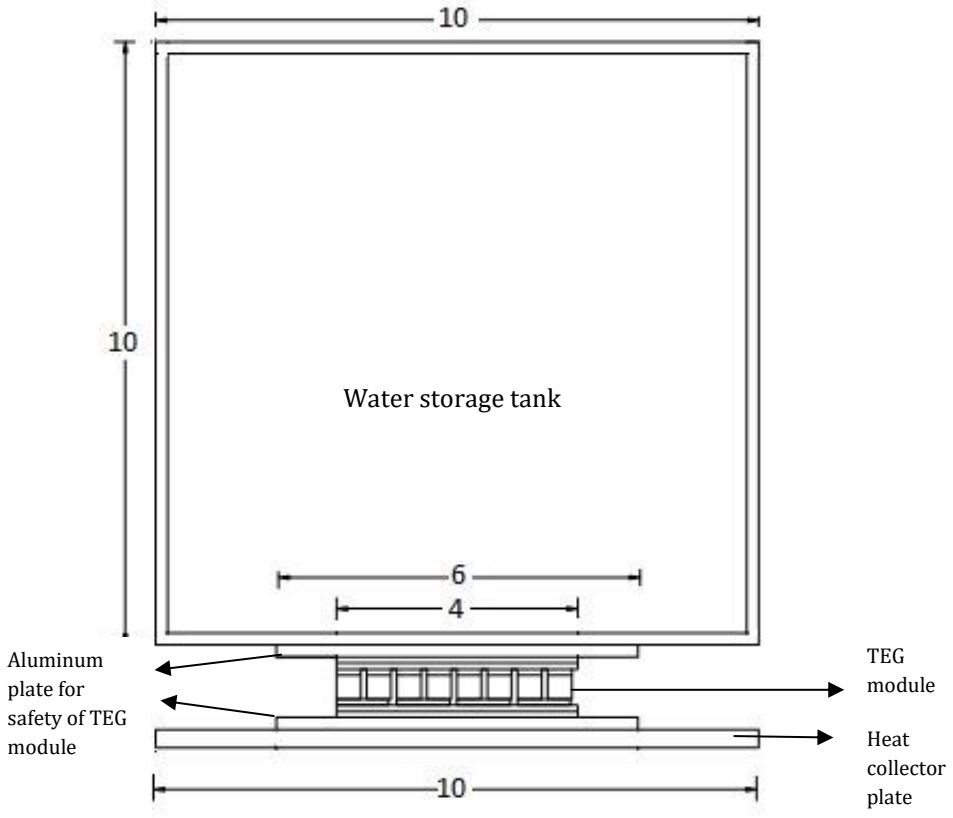

Fig. 3.12 Top view of the TEG assembly (all dimension are in cm)

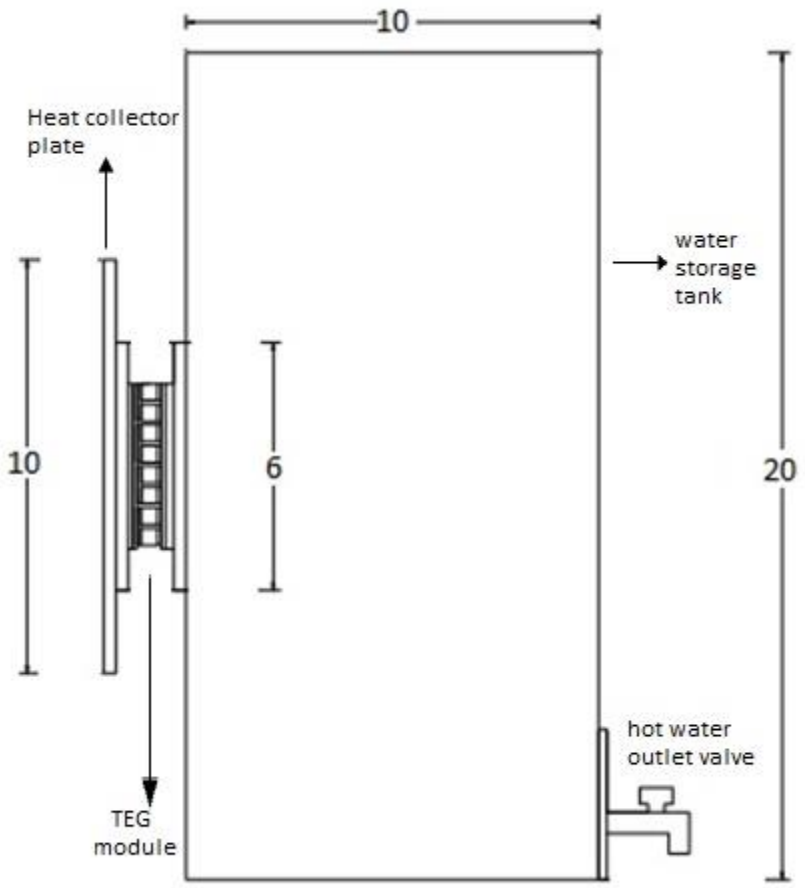

Fig. 3.13 Side view of TEG assembly (all dimension are in cm)

3.11.8. Integration of TEG assembly with improved fixed clay cook stove, *Sukhad*

The combustion chamber of the improved fixed clay stove offered a cylindrical shape of diameter 18cm and height 21cm. The location identified for mounting heat collector plate at angular position of 90º and 9cm above the fuel bed was cut in the dimension of heat collector plate i.e. 10cm × 10cm and the TEG assembly was integrated as shown in Fig. 3.14.

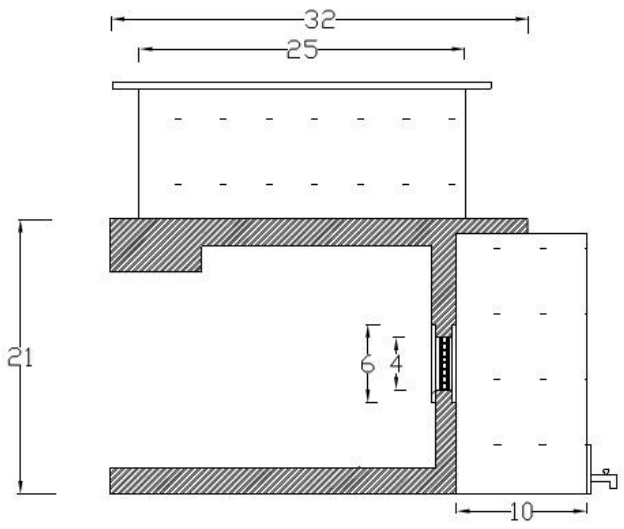

Fig. 3.14 Schematic of experimental set up showing integration of TEG

3.11.9. Experimental test results and discussion of TIFICS

3.11.9.1. Maximum achievable temperature difference for operation of TIFICS

Temperature of 30 tests spreading over an hour of stove operation were averaged and presented in Fig. 3.15 as recorded at four locations (viz., hot side TEG, cold side TEG, flame and ambient). The flame temperature stabilized with some increase beyond initial transient period (~20 min). The maximum recorded flame temperature was 755ºC. Most of the time (>30 min) of stove operation, the flame temperature was between 600 and 750ºC. The maximum temperature recorded at the hot side of the TEG module had been 301ºC which was within the safe limit (330ºC) of TEG as per the TEG manufacturer's specification. The natural convection of water cooling used in the present case resulted a peak temperature of 74ºC at the TEG cold side. It was expected that maintaining the cold side temperature close to ambient temperature would yield higher temperature difference and thus higher power production. In the present case, the cold side temperature increased by more than 40ºC from the ambient temperature. During the starting phase (~20 min) i.e. cold phase of TIFICS, sufficient temperature difference could not be created across the TEG module. However, temperature difference gradually increased after 20 min. The temperature recorded at the hot and cold side of the TEG resulted in sufficient temperature difference to produce electrical power during laboratory tests.

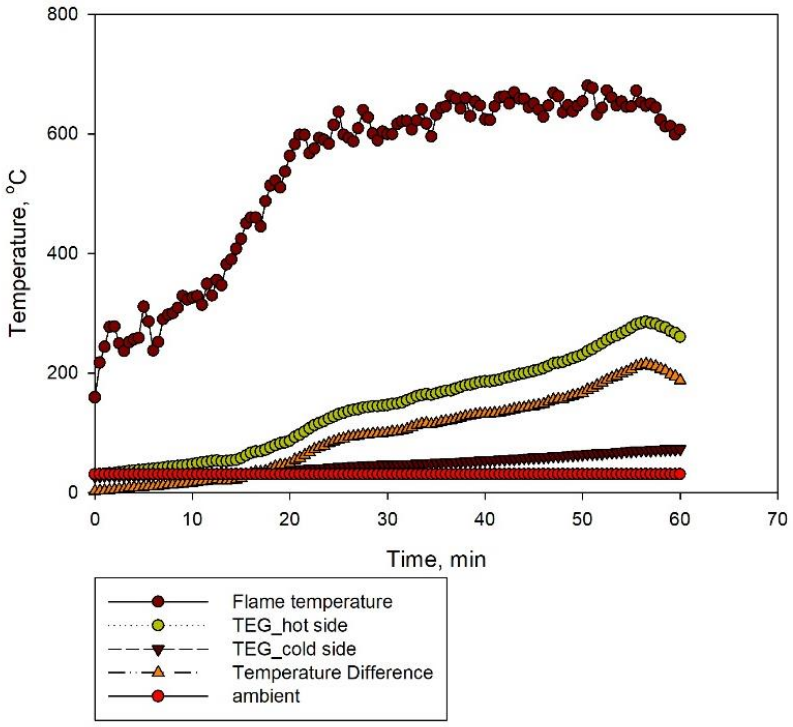

Fig. 3.15 Temperature of flame, ambient, TEG hot side and TEG cold side

3.11.9.2. Performance of TIFICS

In the first mode of operation, the TEG was connected to a matched load. The recorded voltage along with estimated current and power are plotted against corresponding temperature difference across TEG and presented in Fig. 3.16. A linear relationship between power produced and temperature difference was observed which is in good agreement with fundamental theory of thermoelectric principle and results reported in literatures. From the Fig. 3.16, it is observed that about 144ºC of temperature difference across TEG module was required to produce 1W of power. A maximum of 2.7W of power was produced at a temperature difference of 231ºC. The peak load voltage obtained was 4.03V which was lower to operate directly 5V powered applications such as mobile phone charging and LED illumination. The voltage produced was not regulated and was not suitable to operate any applications. External circuit topology such as DC-DC convertor to maintain 4.03V to 5V would be required.

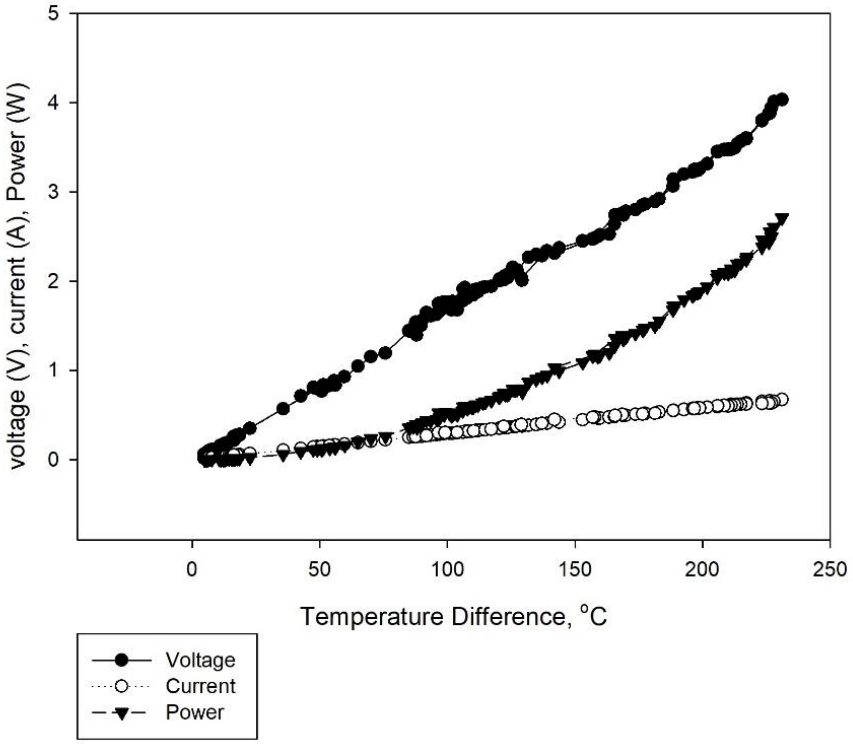

Fig. 3.16. Variation of output power, voltage and current w.r.t. temperature difference across TEG during TIFICS operation

The recorded voltage, estimated current and power are plotted against time for a typical cooking cycle of 1h and is shown in Figure 3.17. The power generation was low (0.03W) during the initial period (~15th min) of test, which might be due to existence of transient heat transfer process. As quantity of firewood supply increased with passage of time, the temperature of the hot side also increased and so did the production of power. The peak power of 2.7W, with load voltage of 4.03V and load current of 0.67A, was recorded at a temperature difference of 231ºC. Towards the end of the cooking cycle, firewood supply was stopped and the temperature at the hot side decreased which resulted in steep fall of voltage, current and power as shown in the Fig. 3.17.

In order to estimate the production of electrical energy over the course of the test, the power vs time curve (Fig 3.17) was integrated mathematically and electrical energy production was estimated to be 1.7W-h.

The result of the present work was compared with some of the reported literatures on TEG integrated cook stove. The power output (2.4W) of the low cost stove-top thermoelectric generator corresponding to 150ºC temperature difference (240ºC hot side) was more than the

TIFICS at identical condition of temperature difference [21]. Similarly, 6W power corresponding to 175ºC temperature difference in a portable cook stove with forced convective air cooling was also substantially higher than the power output of TIFICS under identical condition [22]. Higher power outputs of the earlier TEG integrated stoves than present test results (TIFICS) even at identical temperature difference conditions might be due differences of the design configuration including the provision of forced convection on the cooling sink. However, the addition of fan for forced air or water convection involves consumption of auxiliary power from the TEG system. Moreover, additional cost was involved due to requirements of electrical components. The justification of forced convection at cooling side should be decided based on the net economical gain for a long duration operation, which could not be done in the present investigation.

However, thermal energy stored in the water of the cooling chamber of TIFICS could be considered as a gain because hot water was useful for most of families. It was found that around 1kWh as thermal output was produced in the form of hot water during each 10h of TIFICS operation as an auxiliary output from the waste heat in addition to a peak electrical power output of 2.7W while maintaining 231ºC temperature difference across the TEG module.

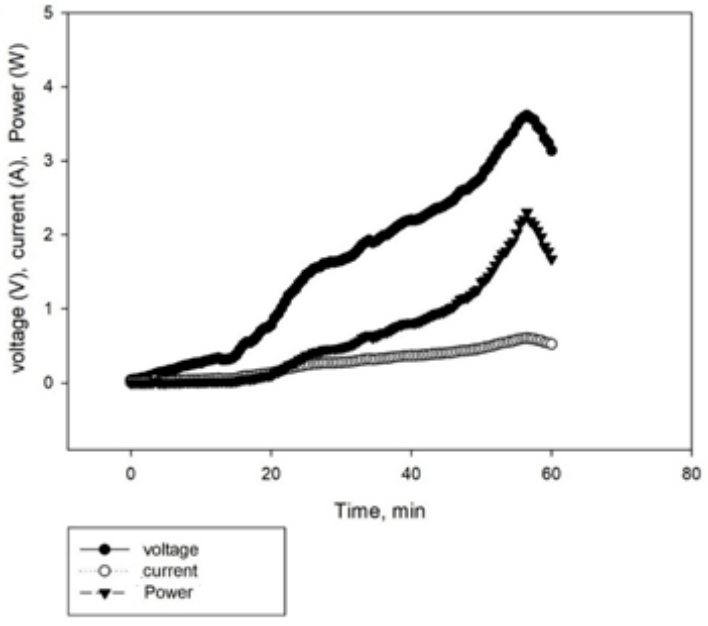

Fig. 3.17 Variation of output power, voltage and current w.r.t. time of TIFICS operation

It is evident from Fig 3.17, that load voltage was less than 1.0V till 20th min of TIFICS operation. Such issues of low voltage were also experienced by earlier researchers working on TEG and addressed by providing DC-DC step up converter [24-29]. A low input (0.9V-5V) with current output of 0.2-0.6A pulse frequency modulation (PFM) controlled DC-DC converter had been used in the present investigation to boost up the voltage requirements for powering the LED bulb (Fig. 3.18). The converter was connected to the output of the TEG in order to get a stable 5V DC supply to operate the LED bulb.

The illumination of bulb through the electrical output of TIFICS is illustrated in Fig. 3.19. It was observed that nearly 15 min of warm up time was required for illumination of the bulb from the start of the stove operation whereas, it remained illuminated beyond 20min making a total of 65 min of illumination for one typical cooking cycle of TIFICS. The late starting and powering beyond stove operation were also experienced by earlier researchers, which could be due to insufficient initial temperature difference and residual heat beyond the fuel supply. A TEG integrated cook stove could power the LED at 27th min of stove operation using a single TG1208-1LS TEG module and could continue to illuminate for 30min even after the fuel feeding was stopped [25].

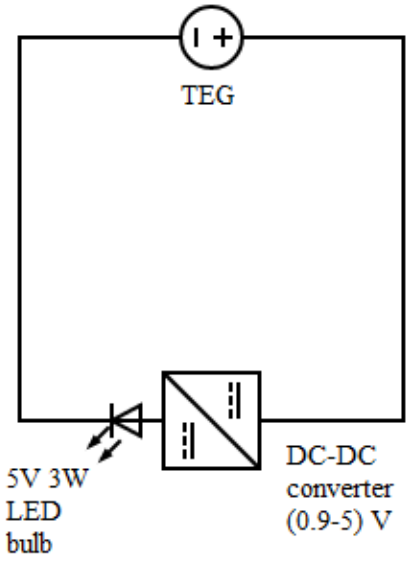

Fig. 3.18. Circuit for 3W bulb illumination

Fig. 3.19 Illumination of workspace using TIFICS

It is important to mention that rather than direct illumination of LED, it is better and more beneficial if power is drawn from a battery charged by TEG. In that way, longer duration of illumination can be achieved (more than 65min) for one cycle of operation. The proceeding section details the charging characteristics of a battery by TIFICS.

There are specific time and duration of operation of cook stove as per the cooking habit of a locality. In general, about 5 to 6h of time was required for cooking purpose throughout a day whereas, illumination requirements were during night only. In order to broaden the utility of TIFICS to enable it to store energy and charge devices such as mobile phone battery as and when required, the technical feasibility of battery charging was tested using TIFICS. However, the selection of the battery was a crucial part. Based on the achieved peak load voltage of 4.03V, battery of operating voltage in that range was selected as reference for battery selection. Five types of batteries were selected and compared as shown in Table 3.6. The specifications were collected from manufacturers and suppliers of these batteries.

Table 3.6 Selection of battery for charging

Sl No.	Battery	Voltage, V	Energy Density ,Wh/L	Operating temperature, ºC	Life Cycle, cycles	Safety	Environment friendly
1	$LiFePO_4$	3.2	220	-20 to 60	>2000	Yes	Yes
2	Lead Acid	2	90	-20 to 40	>200	Yes	No
3	NiCd	1.2	150	-20 to 50	>1000	Yes	No
4	NiMH	3.2	140	-20 to 50	>500	Yes	No
5	$LiCoO_2$	3.7	250	-20 to 60	>500	No	Fair

Lead acid batteries are widely used for its robust nature. However, its low energy density of 90Wh/L make it larger and heavier compared to other batteries. Nickel Metal Hydride (NiMH) batteries are also used for its low cost and low nominal voltage, but when overcharged, NiMH releases hydrogen which is hazardous and thus not environment friendly [52]. Lithium ion cobalt batteries ($LiCoO_2$) in some cases when overcharged can break and lead to combustion and thus not safe for the present study. The energy density of lithium iron phosphate battery ($LiFePO_4$-) is better and such batteries are available in compact shape. $LiFePO_4$ can be kept in a discharged without causing any damage. With high energy density and longer life cycle, safety and for being environment friendly $LiFePO_4$ is selected. In the present work, a 3.2V 2.0Ah battery was selected to be charged by TIFICS.

The battery requires minimum of 3.2V to start charging. However, the TEG voltage recorded was found to under 3.2V at a temperature difference of 190ºC till 55th min of stove operation. As the temperature difference reached beyond 200ºC, the TEG output voltage began to increase above 3.2V. From the Fig. 3.20, it is observed that the battery voltage was at 2.5V till the 55th min of stove operation. However, as the TEG voltage increased beyond 3.2V, the battery followed the TEG voltage. At this stage, i.e., after the 55th min, the temperature difference across the TEG module was recorded to be between 200 and 230ºC and the TEG voltage varied from 3.2V to 4V with current varying from 0.56-0.67A. For 75% of the charging time, the battery voltage stayed between 3.2 and 3.4V. Around 3.7h of continuous stove operation on average was required to fully charge the battery.

The findings can be compared with an earlier work where the battery voltage remained within 3.3-3.4V for 80% of charging time [52].

Thus the feasibility of TIFICS in illuminating and charging a battery was tested. The technological knowhow generated was further aimed to extend in a rural area to investigate

its applicability. For the reason, a battery charging was designed for field testing of TIFICS and is shown in Chapter 4.

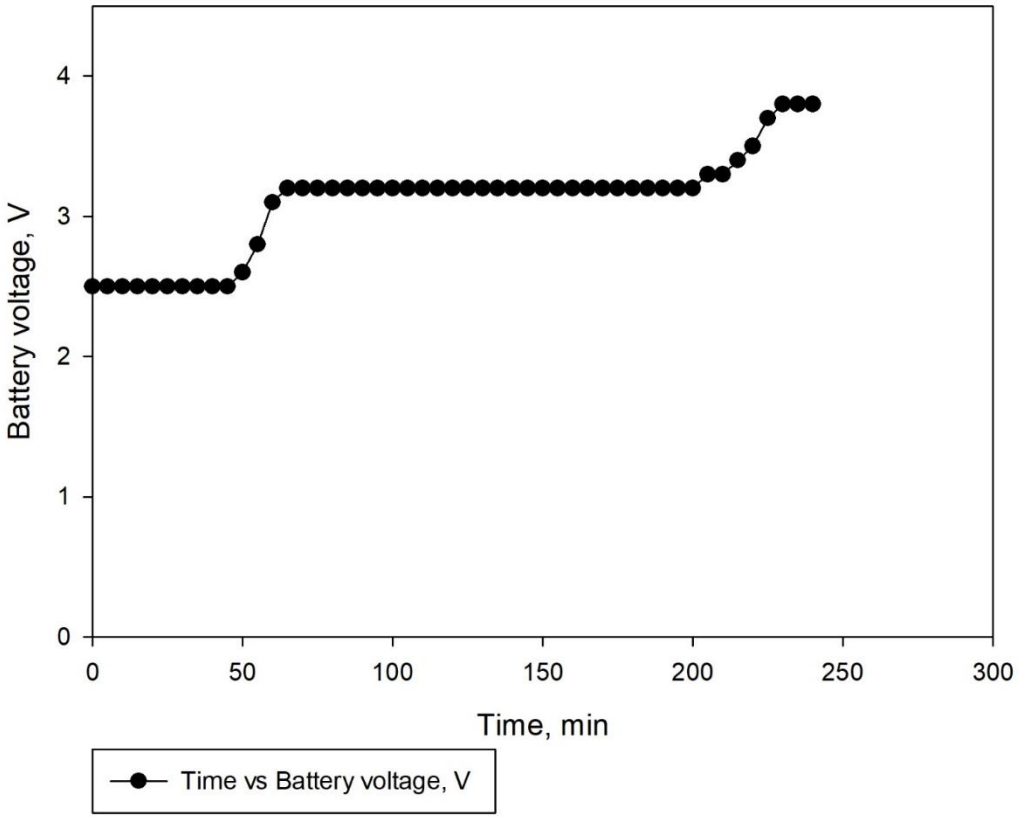

Fig. 3.20 Battery charging characteristics

3.12. Summary

In this chapter, we have specified the objectives, discussed the research methodologies, developed and lab tested a TEG integrated fixed clay stove. This information was new because it was not known earlier for a fixed clay cook stove. New information pertaining to estimation of waste heat for recovery and conversion into electricity, identification of suitable location for TEG, design of TEG assembly and its integrated in a fixed clay improved cook stove was generated which could be beneficial for researchers to explore further in the area. Previous works were limited to portable metallic cook stoves. This particular fixed clay stove is expected to have a preference to a normal cook stove. The technical feasibility of utilizing waste heat and integrating TEG with a fixed clay cook stove was investigated with sufficient electricity to charge a battery and illuminate a LED light. The first objective is accomplished

in the present chapter. The technical feasibility and acceptability of TIFICS in a typical rural area with inadequate access to electricity and solid fuel domination is presented (Objective 2) in Chapter 4. A graphical summary of the present Chapter is illustrated in Fig. 3.21.

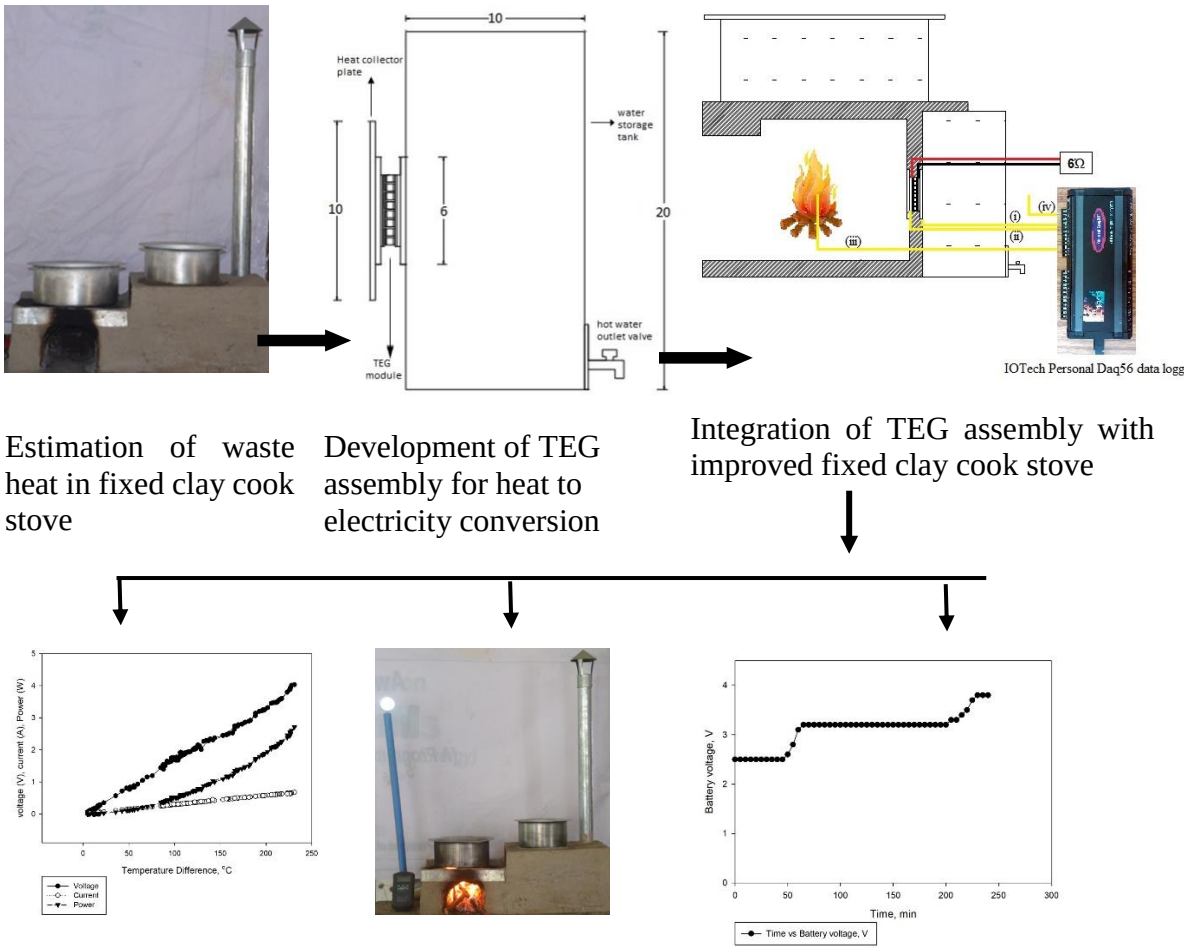

Technical fesibility of integrating TEG with fixed clay stove

Fig. 3.21 Graphical summary of Chapter 3

References

[1] Tyagi, S.K. Pandey, A.K. Sahu, S. Bajala, V. and Rajput, J.P.S. Experimental study and performance evaluation of various cook stove models based on energy and exergy analysis. *Journal of Thermal Analysis and Calorimetry*, 111:1791–1799, 2013.

[2] Sutar, K.B. Singh, R. Karmakar, A. and Rathore, V. Experimental investigation on thermal performance of three natural draft biomass cookstoves. *Energy Efficiency*, 12(3): 749-755, 2019.

[3] Honkalaskar, V.H. Sohoni, M. and Bhandarkar, U.V. Thermo-chemical modelling of a village cookstove for design improvement. Combustion Theory Modelling, 18(3): 414-453, 2014.

[4] NBCI, Cooking energy solutions and sustainable development, Retrieved on 21.08.2017 from https://mnre.gov.in/file-manager/akshay-urja/november-december-2011/EN/24-29.pdf. 2011.

[5] FAO, Food and Agriculture Organization of the United Nations; FAO regional wood energy development programmeme in Asia. Indian improved cookstoves: a compendium. Field document no. 41. Bangkok, Thailand; 1993.

[6] Glance, A. (2015). Energy demand Household Energy 10. TERI Energy and Environment Data Diary and Yearbook (TEDDY) 2014/15: With Complimentary CD, 2076(059), 259.

[7] Venkataraman, C., Sagar, A. D., Habib, G., Lam, N., & Smith, K. R. The Indian national initiative for advanced biomass cookstoves: the benefits of clean combustion. *Energy for Sustainable Development*, 14(2), 63-72, 2010.

[8] Chengappa, C., Edwards, R., Bajpai, R., Shields, K. N., & Smith, K. R. Impact of improved cookstoves on indoor air quality in the Bundelkhand region in India. *Energy for Sustainable Development*, 11(2), 33-44, 2007.

[9] Schreiner, N. H. Performance characteristics and design recommendations for biomass-burning stoves using earthen construction materials, Master's thesis. Department of Environmental Engineering, Michigan Technological University. 2011.

[10] Indian Standard Portable Solid Bio-Mass Cookstove (Chulha) Part 1, Retrieved on 10/01/2017 from http://www.bis.org.in/sf/med/med04_1157c.pdf, 2013.

[11] Gogoi, B., & Baruah, D. C. Steady state heat transfer modelling of solid fuel biomass stove: Part 1. *Energy*, 97:283-295, 2016.

[12] Agenbroad, J. N. A simplified model for understanding natural convection driven biomass cooking stoves, Master's thesis, Colorado State University. 2010.

[13] Agenbroad, J. DeFoort, M. Kirkpatrick, A. and Kreutzer, C. A simplified model for understanding natural convection driven biomass cooking stoves—Part 1: Setup and baseline validation. *Energy for Sustainable Development*, 15(2):160-168, 2011.

[14] Prapas, J. Baumgardner, M. E. Marchese, A. J. Willson, B. and DeFoort, M. Influence of chimneys on combustion characteristics of buoyantly driven biomass stoves. *Energy for sustainable development*, 23: 286-293, 2014.

[15] Bergman, T. L. Incropera, F. P. Lavine, A. S. and DeWitt, D. P. Introduction to heat transfer. John Wiley & Sons.2011.

[16] Holman, J.P. Heat Transfer. The McGraw-Hill Companies Inc; 2010.

[17[Howell, J.R., A catalog of radiation configuration factors, McGraw-Hill, 1982.

[18] Howell, J.R. Menguc, M.P. snf Siegel, R. Thermal radiation heat transfer. CRC press, 2015.

[19] Killander, A., and Bass, J. C. A stove-top generator for cold areas. In *IEEE Fifteenth International Conference on Thermoelectrics* (ICT'96) pages 390-393, Pasadena, California, USA, 1996.

[20] Nuwayhid, R.Y. Shihadeh, A. and Ghaddar, N. Development and testing of a domestic woodstove thermoelectric generator with natural convection cooling. *Energy Conversion and Management*, 46(9-10):1631-1643, 2005.

[21] Lertsatitthanakorn, C. Electrical performance analysis and economic evaluation of combined biomass cook stove thermoelectric (BITE) generator. *Bioresource Technology*, 98(8):1670-1674, 2007.

[22] Champier, D. Bedecarrats, J.P. Rivaletto, M. and Strub, F. Thermoelectric power generation from biomass cook stoves. *Energy*, 35(2):935-942, 2010.

[23] Goudarzi, A.M. Mazandarani, P. Panahi, R. Behsaz, H. Rezania, A. and Rosendahl, LA. Integration of thermoelectric generators and wood stove to produce heat, hot water, and electrical power. *Journal of Electronic Materials*, 42(7):2127-2133, 2013.

[24] Raman, P. Ram, N.K. and Gupta, R. Development, design and performance analysis of a forced draft clean combustion cookstove powered by a thermoelectric generator with multi-utility options. *Energy*, 69:813-825, 2014.

[25] Mal, R. Prasad, R. and Vijay, V.K. Multi-functionality clean biomass cookstove for off-grid areas. *Process Safety and Environment*, 104:85-94, 2016.

[26] O'Shaughnessy, S.M. Deasy, M.J. Doyle, J.V. and Robinson, A.J. Field trial testing of an electricity-producing portable biomass cooking stove in rural Malawi. *Energy for Sustainable Development*, 20:1-10, 2014.

[27] O'Shaughnessy, S.M, Deasy, M.J. Kinsella, C.E. Doyle. J.V. and Robinson. A.J. Small scale electricity generation from a portable biomass cookstove: Prototype design and preliminary results. *Applied Energy*, 102:374-385, 2013.

[28] O'Shaughnessy, S.M. Deasy, M.J. Doyle, J.V. and Robinson, A.J. Adaptive design of a prototype electricity-producing biomass cooking stove. *Energy for Sustainable Development*, 28:41-51, 2015.

[29] O'Shaughnessy, S.M. Deasy, M.J. Doyle, J.V. and Robinson, A.J. Performance analysis of a prototype small scale electricity-producing biomass cooking stove. *Applied energy*, 156: 566-576, 2015.

[30] Nayyeri, M. A. Kianmehr, M. H. Arabhosseini, A. and Hassan-Beygi, S. R. Thermal properties of dairy cattle manure. *International Agrophysics*, 23(4): 359-366, 2009.

[31] Products from Rice husk. Retrieved on 11.04.2019 from http://agropedialabs.iitk.ac.in/agrilore/sites/default/files/Rice_Husk.ppt

[32] Thermal Conductivity of common Materials and Gases, Retrieved on 10.08.2016 from https://www.engineeringtoolbox.com/thermal-conductivity-d_429.html

[33] Specific heat for metals, Retrieved on 10.06.2016 from https://www.engineeringtoolbox.com/specific-heat-metals-d_152.html

[34] Thermal Diffusivity Table, Retrieved on 10.06.2016 from https://www.engineersedge.com/heat_transfer/thermal_diffusivity_table_13953.htm

[35] Ryu, C. Yang, Y. B. Khor, A. Yates, N. E. Sharifi, V. N. and Swithenbank, J. Effect of fuel properties on biomass combustion: part I. Experiments—fuel type, equivalence ratio and particle size. *Fuel*, 85(7): 1039-1046, 2006.

[36] Yang, Y. B. Ryu, C. Khor, A. Yates, N. E. Sharifi, V. N. and Swithenbank, J. Effect of fuel properties on biomass combustion. Part II. Modelling approach—identification of the controlling factors. *Fuel*, 84(16), 2116-2130, 2005.

[37] HZ-2 Thermoelectric Module, Retrieved on 10.2.2016 from https://hi-z.com/product/hz-2-thermoelectric-module/

[38] HZ-9 Thermoelectric Module, Retrieved on 10.2.2016 from https://hi-z.com/product/hz-9-thermoelectric-module/

[39] TEP1-1264-1.5. Retrieved on 10.01.2016 from http://www.thermonamic.com/TEP1-1264-1.5-English.pdf

[40] TEC12706, Retrieved on 10.01.2016 from https://peltiermodules.com/peltier.datasheet/TEC1-12706.pdf

[41] TEG1-4199-5.3, Retrieved on 10.01.2016 from https://tecteg.com/product/teg1-4199-5-3/

[42] TEG1-12610-4.3, Retrieved on 10.01.2016 from https://tecteg.com/product/ teg1-12610-4.3/

[43] TEG1-12610-5.1. Retrieved on 10.01.2016 from https://tecteg.com/product/ teg1-12610-5.1/

[44] TEG1-1268-4.3. Retrieved on 10.01.2016 from https://tecteg.com/product/ teg1-1268-4.3/

[45] TEG1-1263-4.3. Retrieved on 10.01.2016 from https://tecteg.com/product/ teg1-1263-4.3/

[46] TEP1-12635-3.4. Retrieved on 10.01.2016 from http://www.thermonamic.com/ TEP1-12635-3.4-English.pdf

[47] TEP1-1265 1.5. Retrieved on 10.01.2016 from http://www.thermonamic.com/ TEP1-1265 1.5-English.pdf

[48] TEP1-1264 3.4. Retrieved on 10.01.2016 from http://www.thermonamic.com/ TEP1-1264 3.4-English.pdf

[49] TEG1B-12610-5.1. Retrieved on 10.01.2016 from https://tecteg.com/product/ teg1- b-12610-5.1/

[50] TEP1-1994-3.5. Retrieved on 10.01.2016 from http://www.thermonamic.com/ TEP1-1994-3.5-English.pdf

[51] TEG2-07025HT-SS. Retrieved on 10.01.2016 from https://tecteg.com/product/teg2-07025ht-ss-graphite-both-sides/

[52] Kinsella, C. E. O'Shaughnessy, S. M. Deasy, M. J. Duffy, M., and Robinson, A. J. Battery charging considerations in small scale electricity generation from a thermoelectric module. *Applied Energy*, 114, 80-90, 2014.